Perturbation of ATP6V0A1 as a Driver and Druggable Target for Renal Proximal Tubular Cellular Injury in Nephropathic Cystinosis

Swastika Sur[1], Maggie Kerwin[1], Silvia Pineda[1,2], Poonam Sansanwal[1], Tara K. Sigdel[1], Marina Sirota[2] and Minnie M. Sarwal[1]

[1]Division of Multi-Organ Transplantation, Department of Surgery, University of California, San Francisco

[2]Bakar Computational Health Sciences Institute, University of California San Francisco, San Francisco, California, USA.

Corresponding Author: Minnie M. Sarwal, MD, PhD, Medical Director, Kidney and Pancreas Transplant Program, Division of Multi-Organ Transplantation, Department of Surgery, University of California, San Francisco, 513 Parnassus Ave, Med Sciences Bldg, Room S1268, San Francisco, CA 94143 (minnie.sarwal@ucsf.edu)

Running Title: ATP6V0A1 in Nephropathic Cystinosis

Key words: Cystinosis, kidney disease, genetic renal, ESRD, autophagy, CKD

Abstract

Understanding the unique susceptibility of the human kidney to pH dysfunction and injury in cystinosis is paramount to develop new therapies to preserve renal function. Renal proximal tubular epithelial cells (RPTECs) and fibroblasts, isolated from patients with cystinosis were transcriptionally profiled. Lysosomal fractionation, immunoblotting, confocal microscopy, intracellular pH, TEM, mitochondrial stress test, and membrane integrity assays were performed for validation. CRISPR, *CTNS* $^{-/-}$ RPTECs were generated. A new compound, Astaxanthin (ATX), was evaluated for rescue of the *CTNS* $^{-/-}$ phenotype. Alterations in cell stress, pH, autophagic turnover, and mitochondrial energetics, highlighted key changes in the vacuolar (V)-ATPases in patient derived and *CTNS*$^{-/-}$ RPTECs. ATP6V0A1 was significantly downregulated in cystinosis and highly co-regulated with loss of *CTNS*. Overexpression of ATP6V0A1 rescued cell stress and mitochondrial function. Treatment of *CTNS* $^{-/-}$ RPTECs with ATX, induced ATP6V0A1 expression and the resulting rescue of the RPTE cell and mitochondrial injury.

In conclusion, our exploratory transcriptional and in vitro cellular and functional studies confirm that loss of cystinosin in RPTEC, results in a reduction in ATP6V0A1 expression, with changes in intracellular pH, mitochondrial integrity, mitochondrial function, and autophagosome-lysosome clearance. ATX can rescue the cystinotic RPTEC injury, at least partially mediated by upregulating ATP6V0A1 expression. The availability of ATX as a well-tolerated oral supplement, offers its further clinical evaluation as a potential novel therapeutic to limit renal tubular injury in cystinosis, independent of cysteine depletion alone.

39 **INTRODUCTION**

40 Lysosomal storage diseases (LSD) form a significant subgroup of inherited metabolic disorders (1-4),
41 with an incidence of more than 1:5,000 live births (3). Cystinosis is a rare autosomal recessive LSD,
42 caused by mutations in the *CTNS* gene, encoding lysosomal membrane
43 transporter cystinosin (5). Deficiency of cystinosin results in lysosomal cystine accumulation and cystine
44 crystal formation in virtually all tissues and organs (6). The kidney is the first organ affected functionally,
45 despite lysosomal cystine loading in multiple tissues and organ systems. Based on severity and age at
46 onset of renal injury, cystinosis is phenotypically classified into nephropathic/infantile
47 (OMIM219800)(7), juvenile (OMIM 219900)(8) and ocular (OMIM 219750)(9). The most severe form is
48 nephropathic/infantile cystinosis, characterized by the development of renal Fanconi syndrome and
49 glomerular dysfunction, resulting in end-stage renal disease (ESRD) by 10 years of age, extendable to the
50 second decade of life with cystine depletion therapy (10, 11). Nevertheless, persistent Fanconi and
51 progressive renal failure remains a reality for these patients, despite robust adherence with cystine
52 depletion therapies (12). These observations suggest that cystinosin or other key molecular perturbations
53 impact renal tubular integrity and function besides cystine transport (13).

54 Though associative functional roles for cystinosin have been identified, including mammalian target of
55 rapamycin (mTOR) signaling (14-16), defective autophagy, flawed clearance of damaged mitochondria
56 by disrupted mitophagy (17, 18), lysosomal biogenesis (19), abnormal tight junction-associated signaling
57 (17), vesicular transport defects, and increased endoplasmic reticulum (ER) stress (20), the underlying
58 drivers for these injuries have not been well identified, resulting in a paucity of new therapies to improve
59 outcomes in nephropathic cystinosis. Furthermore, we and others have shown that renal biopsies from
60 patients with nephropathic cystinosis reveal morphologically abnormal mitochondria and mitophagy with
61 autophagic vacuoles, reduced mitochondrial numbers (18, 21), increased ROS production (17) and
62 reduced lysosomal enzyme activity (22).

63 We hypothesized that defective lysosomal clearance may be a pivotal cause of the altered function of
64 renal proximal tubular epithelial cells (RPTECs). Given lysosomes ubiquitous presence in all tissues and
65 organ-systems, we hypothesized that a comparison of transcriptional profiles of renal and extra-renal
66 tissues from patients with nephropathic cystinosis would shed light on the unique lysosomal changes in
67 the human kidney responsible for both the renal tubular injury in Fanconi and the progressive renal
68 tubular injury resulting in ESRD. With this in mind, we investigated whole-genome expression profiles in
69 paired RPTECs (21, 23) (isolated from patient urine samples) and fibroblasts (21) (isolated from the same
70 patient skin biopsies) from cystinosis patients and healthy age- and gender-matched controls. We
71 identified dysregulation of the V-ATPase multigene family, specifically ATP6V0A1, only in cystinotic
72 RPTECs and not normal RPTECs and fibroblasts or cystinotic fibroblasts. To further study the structural
73 and functional consequences of ATP6V0A1 deficiency, a CRISPR-mediated CTNS-knock-out ($CTNS^{-/-}$
74) immortalized RPTEC line was generated as an *in-vitro* model that mimicked structural and functional
75 changes seen in patient-derived RPTECs. The $CTNS^{-/-}$ RPTECs also demonstrated
76 ATP6V0A1 downregulation, resulting in significant functional (loss of acidic lysosomal pH, decreased
77 autophagic flux, compromised mitochondrial ATP-production) and structural consequences (increased
78 vacuolization, lack of mitochondrial cristae, reduced number of mitochondria, ER-stress and intracellular
79 lipid droplet (LD) formation). Further, overexpression of ATP6V0A1 in $CTNS^{-/-}$ RPTECs and treatment
80 with novel drug ATX that increases production of cellular ATP6V0A1, identified from a custom FDA-
81 drug database generated by our group, partially rescued the nephropathic RPTEC phenotype (24). ATX is
82 a xanthophyll carotenoid occurring in a wide variety of organisms. ATX is reported to have the highest
83 known antioxidant activity (25), and has proven to have various anti-inflammatory, anti-tumoral,
84 immunomodulatory, anti-cancer, and cytoprotective activities both *in vivo* and *in vitro* (26-29). For the
85 first time, we utilized ATX to evaluate its potential protective effect against cystinosis-induced lysosomal
86 and mitochondrial dysfunction. Our findings lead us to believe that ATP6V0A1 not only presents as a
87 candidate target for therapy, but that ATX has the potential to be repurposed as a treatment for
88 the renal pathology in nephropathic cystinosis that persists despite current cystine depletion therapies.

89

90 **RESULTS**

91

92 **Global Transcriptional Changes in Cystinotic RPTEC Affect Lysosomal and Mitochondrial**

93 **Pathways**

94 Performed genome wide transcriptional profiling of normal and cystinotic RPTECs and skin fibroblasts
95 with and without CDME (**Figure 2**). The genetic anomaly in cystinosis (mutation of the cystine:proton
96 transporter) is quite heterogeneous with more than 140 mutations found (13). This heterogeneity affects
97 the phenotype of the disease quite significantly. With this in mind all 8 patients from whom the cells were
98 obtained had the same 57kb mutation (30). Normal CDME loaded RPTECs and fibroblasts did not
99 transcriptionally mimic the cystinotic phenotype suggesting that CDME loading is a poor surrogate *in*
100 *vitro* model to study cystinosis tissue injury despite much of earlier research in cystinosis using CDME
101 loading as an in vitro mimic of RPTEC cystinosis in vivo disease **(Fig. 2B-C). Figure 2B and 2E**
102 highlight marked transcriptional differences between cystinotic RPTECs and fibroblasts from the same
103 individual, showing that most of the transcriptional changes, as expected, were tissue specific.
104 Nevertheless, some overlapping genes are significantly dysregulated in both cystinotic RPTECs (n=1,926;
105 FDR<0.05) and fibroblasts (n=745; FDR<0.05), with 219 overlapping genes associated with DNA
106 integrity loss and damage. Further analysis identified that certain molecular pathway were highly enriched
107 (31) only in the kidney, and 11 significant pathway modules were found to be unique
108 to cystinotic RPTECs alone (**Figure 2D, 2E**). **Figure 2E** shows cystinotic RPTEC specific pathways,
109 inclusive of significantly reduced clusterin expression, reported previously by our group (23), and
110 alterations in nuclear-encoded mitochondrial genes, and multiple V-ATPase genes involved in lysosomal
111 acidification (32-35) ((hypergeometric enrichment P<0.001). Nine lysosomal v-ATPases were
112 significantly downregulated in cystinotic RPTECs, some of which play important roles in proximal tubule
113 (PT) H^+ secretion to support reabsorption of luminal HCO_3^-, apical endocytosis (36, 37) and may cause

114 PT acidosis (38). The most significant member of the V-ATPase gene family was ATP6V0A1 (**Figure**
115 **2E**), hence further attention was focused on this particular gene.

116

117 **CRISPR-Cas9 Mediated Immortalized CTNS$^{-/-}$ RPTECs**

118 Given that CDME loading of RPTECs was observed to not be a replicative model of diseased RPTECs
119 cultured from cystinosis patients, we generated and validated a CRIPR based *CTNS* gene knockout *in-*
120 *vitro* model of RPTEC injury. CRISPR-Cas9 technology was adapted to generate a complete knockout of
121 *CTNS* gene (CTNS$^{-/-}$) in human immortalized (HuIm) RPTECs (**Figure 3)** with 95% efficiency.
122 Validation by HPLC-MS/MS showed a significant increase in cystine accumulation in CTNS$^{-/-}$ RPTECs
123 **(Figure 3C)**, similar to intracellular cystine accumulation found in cystinosis patients (5-6 nmol/mg
124 protein).

125

126 **Loss of Cystinosin and ATP6V0A1 Expression and Loss of Acidic pH**

127 Compared to controls, ATP6V0A1 protein expression was significantly decreased in both
128 primary cystinotic and CTNS$^{-/-}$ cells with an eight-fold reduction in isolated lysosomal fractions (**Figure**
129 **4A-C**). Confocal imaging showed reduced immunopositivity for both LAMP2 (lysosomal marker) and
130 ATP6V0A1 in cystinotic RPTECs (**Figure 4E**), with clear expression of both in normal lysosomes. V-
131 ATPases are highly conserved, ubiquitously expressed, and required for organelle acidification and ATP-
132 driven proton transport. **Figure 4F-G** shows a significant reduction in intracellular acidic pH in cystinotic
133 (pH=5 vs normal RPTEC pH of 4.2) and CTNS$^{-/-}$ RPTEC (pH=6.6 vs control human immortalized
134 RPTECs pH of 5.8). An increase of ~0.8 pH units in cystinotic RPTEC translates into a 6.3 fold
135 difference in hydrogen ions, large enough to disturb normal RPTECs cellular function.

136

137 **Lack of Cystinosin and ATP6V0A1 Reduced Autophagosome Turnover and mTORC1 Activity**

138 In prior studies (18, 21) we showed increased autophagy or reduced autophagosome turnover in cystinotic
139 cells. **Figure 5A** illustrates enhanced formation of LC3B-positive puncta in cystinotic RPTECs. LC3B-
140 puncta are a hallmark of compromised V-ATPase function in autophagosome clearance, often induced by
141 treating cells with V-ATPase inhibitor Bafilomycin. We additionally observed reduced immunopositivity
142 towards phosphorylated-p70S6 kinase protein, a direct downstream substrate of mTORC1 (**Figure 5B**)
143 and common marker of mTOR activity.
144
145 **Lack of Cystinosin and ATP6V0A1 Compromised Mitochondrial Function**
146 The cell mito-stress test with Agilent Seahorse XFe instrument assessed Mitochondrial function in CTNS^{-}
147 $^{/-}$ and cystinotic RPTECs. Both cystinotic and CTNS$^{-/-}$ RPTECs exhibited similar patterns of compromised
148 mitochondrial function (**Figure 6**), with significantly decreased basal and maximal respiration and ATP
149 production compared to controls. The OCR linked to proton leak and cells spare respiratory capacity was
150 significantly lost in cystinotic cells. However, non-mitochondrial oxygen consumption did not
151 significantly change in cystinotic or CTNS$^{-/-}$ RPTECs. There was a substantial increase in OCR linked to
152 proton leak in normal cells, indicating that normal cells when injected with inhibitors have higher proton
153 leak than the diseased cells with inhibitors. This observation indicates damaged mitochondrial inner
154 membrane in cystinotic cells to begin with, as injecting inhibitors did not make much difference to
155 already compromised mitochondria. The findings suggest that decline in total ATP production can be
156 largely attributed to decreased mitochondrial ATP production.
157
158 **ATP6V0A1 Overexpression Improved Autophagosome Turnover and Mitochondrial Function**
159 Since most genes crucial for mitochondrial ATP-generation were downregulated in cystinotic RPTEC, we
160 hypothesized that even without functional cystinosin, overexpressing ATP6V0A1 would positively affect
161 mitochondrial function and autophagosome turnover. We overexpressed ATP6V0A1 in CTNS$^{-/-}$ RPTECs
162 and observed reduced LC3-II accumulation (**Figure 7A**) indicating either reduced autophagy or increased
163 autophagosome turnover. In addition, study of mitochondrial function (seahorse) revealed increased

164 mitochondrial basal respiration, indicating an increased energy demand, and a trend of increased
165 respiratory capacity and mitochondrial ATP-production with ATP6V0A1 overexpression (**Figure 7B**).
166 These results suggest that vacuolar pH is indeed an important determinant in cystinosis pathophysiology,
167 but further work is needed to fully elucidate how these changes also improve mitochondrial oxidative
168 phosphorylation. Importantly, preventing the decline in vacuolar acidity, through ATP6V0A1
169 overexpression, was sufficient for improving autophagosome turnover.

170 **Overexpression of ATP6V0A1 Rescued Morphologic Alterations**

171 TEM characterized cellular morphologic aberrations in cystinotic, CTNS$^{-/-}$, and CTNS$^{-/-}$+ATP6V0A1
172 overexpressed RPTECs (**Figure 7C).** We observed a significant increase in autophagic vacuoles (AV),
173 decrease in mitochondrial number with few or no cristae, swollen ER and LD presence within CTNS$^{-/-}$
174 RPTECs, similar to cystinotic RPTEC. Similar to control RPTECs, ATP6V0A1 overexpression
175 significantly reduced AV (**Figure 7D-F**) and increased mitochondria number with well-preserved cristae.
176 Nevertheless, overexpression did not affect intracellular LD accumulation.

177 **ATX Increases ATP6V0A1 Expression Improving Autophagosome Turnover and Mitochondrial**
178 **Dysfunction**

179 To evaluate whether ATX affects cystinosis dysregulated pathways, we initially investigated our target
180 gene of interest, ATP6V0A1. Interestingly, ATX pretreatment increased ATP6V0A1 protein expression
181 in CTNS$^{-/-}$ RPTECs **(Figure 8B)**. To evaluate whether ATX could improve autophagic clearance via
182 upregulating ATP6V0A1, LC3-II levels were measured and showed significant reduction of LC3-II with
183 ATX **(Figure 8B)**. Similar findings between ATP6V0A1 overexpression and ATX treatment suggest
184 ATX may ameliorate the impaired autophagy phenotype occurring in cystinotic RPTEC via regulating
185 ATP6V0A1 expression.

186 Using the JC-1 probe, we measured ΔΨm since its decrease is a quintessential event in the early stages of
187 apoptosis. Compared to control, CTNS$^{-/-}$ RPTEC had a significant decrease ($p<0.04$) in the JC-1 ratio of
188 aggregates (590nm) to monomers (530nm) indicating a significant loss in ΔΨm, whereas ATX treatment
189 rescued ΔΨm **(Figure 8A)**, suggesting ATX's protective role in maintaining mitochondrial integrity in
190 CTNS$^{-/-}$ RPTEC. Western blot analysis of pro-apoptotic, p53, demonstrated significantly increased
191 expression in CTNS$^{-/-}$ RPTECs which was significantly reduced with ATX pretreatment (**Figure 8B**).
192 MitoSox, a mitochondrial selective ROS detector, was used to measure mitochondrial-mediated ROS
193 production and WST-1 was used to normalize cell viability. **Figure 8C** shows significantly increased
194 ROS production in CTNS$^{-/-}$ RPTEC ($p<0.0001$) which was rescued with ATX treatment, suggesting
195 ATX's potent antioxidant capacity and ability to improve mitochondrial function.

196 **Figure 8D** shows a schematic overview delineating processes occurring in cystinotic RPTECs
197 with/without ATP6V0A1 overexpression and ATX treatment. Based on our findings, we propose that
198 cystinosin loss downregulates ATP6V0A1, resulting in acidic lysosomal pH loss and adversely modulated
199 mitochondrial function and lifespan in cystinotic RPTECs (**Figure 1B**).
200
201 **DISCUSSION**
202
203 Despite whole body cystine loading, cystinosis predominantly affects the human kidney, causing the renal
204 Fanconi syndrome soon after birth, followed by progressive renal damage, slowed but not avoided by
205 cystine depleting therapies (10, 39). In this study, we identify key and unique disruptions in lysosomal
206 pathways in RPTECs harvested from patients with nephropathic cystinosis, not observed in normal
207 RPTECs nor paired skin fibroblasts from the same cystinosis patients. To assess and cross-validate the
208 structural and functional impact of these unique lysosomal changes in human cystinotic RPTECs, we
209 generated a CTNS$^{-/-}$ *in vitro* HuIm RPTEC cystinosis model to establish a key link between *CTNS* and
210 lysosomal *ATP6V0A1,* to explain for the first time, a potential connection between the early occurrence of

211 a lysosomal acidification defect in renal Fanconi syndrome and progressive structural and functional loss
212 of renal reserve and function. We also utilized our transcriptional data to identify drugs with strong anti-
213 oxidant potential using inferred drug-design using a collated FDA-drug functional database that was
214 originally created to study pre-term birth (24), but preliminary studies (data not shown) with some of
215 these compounds did not reveal in phenotype rescue of RPTECs. ATX was selected from the literature
216 based on its known strong anti-oxidant properties, and was the only agent that provided recovery of the
217 specific RPTEC injury phenotype in cystinosis, over and above any changes related to cystine depletion
218 alone.
219
220 Transcriptional microarray analysis identified that the majority of the genes affected in cystinosis belong
221 to one large cluster, crucial for normal lysosomal and mitochondrial function. We identified ATP6V0A1
222 as the topmost gene downregulated in cystinotic RPTECs, which was also found to have a role in multiple
223 cystinosis-related dysregulated pathways in our dataset. Our data indicates that absence of functional
224 cystinosin downregulates ATP6V0A1 resulting in – loss of acidic pH, decreased autophagy flux,
225 increased autophagosome accumulation, loss of mTORC1 activity, and compromised mitochondrial
226 structure and function, collectively suggesting a possible mechanistic explanation for the progression of
227 PT dysfunction in cystinosis. Interestingly, all these pathophysiologies are known to be compromised in
228 cystinotic RPTECs and are not recovered by cysteamine. Partial recovery of the cystinotic phenotype was
229 observed by overexpressing ATP6V0A1. However, a notable finding in our study is that ATX treatment
230 of $CTNS^{-/-}$ RPTEC rescued ATP6V0A1 levels, enhanced autophagosomal turnover, improved cystinosis-
231 induced mitochondrial dysfunction and rescued mitochondrial membrane potential. The rescue pattern of
232 ATX in $CTNS^{-/-}$ RPTECs is similar to the outcome observed when we overexpressed ATP6V0A1 in these
233 cells. This suggests the ability of ATX to improve on cystinosis-associated pathophysiology in RPTECs
234 may be in part due to its ability to increase ATP6V0A1 expression and in turn improve autophagy
235 turnover and mitochondrial function, which are compromised in $CTNS^{-/-}$ RPTECs. In experimental
236 models of disease, ATX has been shown to regulate autophagy by regulating signaling pathways,

237 including the mitogen-activated protein kinase (MAPK) (40), AMP-activated protein kinase (AMPK)
238 (41), and cellular homolog of murine thymoma virus akt8 oncogene (Akt) (42-46). ATX activates AMPK
239 signaling to promote autophagy by inhibiting mTOR pathway (41). ATX reduces apoptotic cell death by
240 upregulating phosphorylated (p)-Phosphoinositide 3-kinases (PI3K) and p-Akt, resulting in increased cell
241 proliferation and improved cell potency (42-46). ATX inhibits pro-apoptotic and pro-autophagic proteins,
242 by inhibiting cerulein mediated increased LC3 expression. In addition, ATX can inhibit inflammation and
243 autophagy by inhibiting the JAK/STAT3 pathway (47). Cytoprotective effects of ATX under stressors are
244 mediated via MAPKs, particularly, by the inhibition of JNK1/2 activation (48). By blocking p38
245 activation, ATX suppresses apoptosis and ameliorates oxidative stress, ER stress, and mitochondrial
246 dysfunction (49-52). In MIN6 β-cells, ATX inhibits JNK1/2 activation and reduces inflammatory ER
247 stress (53, 54). Cumulatively, these studies establishes ATX as a promising therapeutic agent for the
248 treatment of a wide variety of diseases by regulating autophagy. ATX aids in enhanced insulin-stimulated
249 GLUT4 translocation to the plasma membrane by positively affecting the actin-cytoskeleton re-modeling
250 (55, 56). Based on the research, one may speculate that ATX may have similar role in translocating V-
251 ATPase transporter protein to the lysosomal/organelle surface, regulating the pH and autophagy in CTNS^{-}
252 $^{/-}$ RPTECs. However, further studies are warranted to understand the protective mechanism of ATX in
253 CTNS$^{-/-}$ RPTECs.

254 V-ATPases plays a critical role in acidification of organelles within the endocytic, lysosomal, and
255 secretory pathways and are required for ATP-driven proton transport across membranes (57, 58). In yeast
256 and humans, lack of lysosomal acidic pH impaired lysosomal degradation, resulting in autophagosome-
257 filled lysosomes (59, 60). An elevation by 0.2-0.3 pH units in lysosome was linked to a reduction in the
258 pH-dependent cleavage, and chronic changes in autophagy and degradation, whereas re-acidification of
259 the lysosomes with cAMP reversed these changes (59). Our study revealed that absence of functional
260 cystinosin downregulates ATP6V0A1 resulting in less acidic lysosomal pH in cystinotic RPTECs. We are

261 the first to show that absence of cystinosin affects V-ATPase expression and the acidic pH in the
262 endolysosomal system.

263 There are a few limitations of these studies, inherent mostly to the nature of human studies, where
264 experimental controls cannot be tightly imposed. The fact that cysteamine treatment does not reverse
265 Fanconi syndrome could also mean that lysosomal cystine caused irreversible tubular cell damage or
266 death prior to a year of age when cysteamine treatment generally begins. There is a report of preservation
267 of some renal tubular function when cysteamine was initiated just after birth due to early diagnosis based
268 upon an affected sibling, but even this patient went into ESRD in the second decade of life (61, 62). We
269 also acknowledge that our RPTECs were exposed to CDME for only 30 minutes, after which they began
270 to lose cystine from their lysosomes because of their normal contingent of cystinosin (63). Regardless of
271 how long after loading the cells were harvested, the exposure of the loaded cells to increased lysosomal
272 cystine could not be comparable to longstanding exposure of the knock-out cells to lysosomal cystine.
273 This also explains the very different transcriptional profiles of these cells in this study. We also noted the
274 loss of some epithelial markers in the patient derived RPTECs, which may have occurred with time but is
275 less relevant to this paper as we are looking at a focused pathway in nephropathic cystinosis. We
276 recognized the need for other cell lines that closely mimics the cystinosis-mediated renal pathology;
277 hence, we created the CRISPR-mediated $CTNS^{-/-}$ RPTECs. Nevertheless, we believe that urine RPTECs
278 harvested from patients and the $CTNS^{-/-}$ model system provide closer mimics of the human disease
279 phenotype, and hence adjusts for this limitation of understanding the molecular injury pathways in
280 cystinotic RPTECs. We also acknowledge that despite proposed mechanisms of ATP6V0A1 in this study,
281 it is not possible to conclusively tell if cystinosin deficiency causes lysosomal cystine storage that
282 changes autophagosome morphology and results in cellular expression changes that include
283 downregulation of ATP6V0A1 (RNA and protein) in this study. Additional studies are underway to
284 evaluate the transcriptional regulation of ATP6V0A1 in cystinosis and if any further changes to
285 ATP6V0A1 expression will occur when the $CTNS^{-/-}$ cells are chronically cysteamine treated. A major

286 finding in this paper is that these abnormalities are present in RPTEC cells, but not fibroblasts, and we
287 believe that some of this difference is due to the unique changes in many V-ATPases, many of which are
288 tissue specific in expression This study was not designed to study other tissues which can also display
289 significant injuries, e.g. retina, esophagus, skeletal muscle, CNS, endocrine tissues, and it is possibly that
290 minor and slower onset of functional perturbations in these other organs largely relate to the intra-cellular
291 cysteine accumulation in lysosomes of these organelles, while the specific V-ATPase changes seen in
292 kidney, and not seen in fibroblasts, are also not seen in these other organ systems. Nevertheless, this is
293 purely hypothetical at this time. Similarly, further work is underway to understand how the slow
294 evolution of the disease (~10 years for native renal failure) is fully explained when the major flaw in
295 lysosomal acidification and aberrant autophagy and energy production is present from birth. It is possible
296 there is failure of compensatory mechanisms in the kidney over time, that preserve renal function, until
297 greater loss of functional renal reserve over time.

298 In yeast, decline of lysosomal acidity reduces pH-dependent amino acid storage in the vacuolar lumen
299 causing mitochondrial dysfunction followed by fragmentation and aggregation (60). We also recognize
300 that as the pH of the lysosomes is increased with loss of cystinosin, it would influence lysosomal
301 degradation of proteins. We are currently planning additional experiments to study lysosomal
302 degradation, and how this can be impacted further by treatment with ATX.

303 V-ATPases are needed for ATP-driven proton transport across membranes (57), which explains
304 significant downregulation of several amino acid and metabolite transporters, including SLC17A1,
305 SLC17A3, SLC17A5, SLC3A1 and SLC7A7 (**Supplemental Figure 1**) in cystinotic RPTECs. These
306 findings were a little surprising as there is no clear explanation why sialic acid transporters would be
307 affected and the clinical impact of this perturbation, which requires additional study. We conducted a
308 real-time study on live mitochondria and showed that lack of cystinosin induced damaged morphology
309 while also decreasing number, basal, maximal, and spare respiratory capacity, and ATP production in the
310 diseased cells. This can also be due to inactive mTORC1 that may inhibit mitochondrial biogenesis in

311 cystinotic cells **(64)**. Overexpression of ATP6V0A1 in CTNS$^{-/-}$ cells partially rescued this cystinotic
312 phenotype.

313 Alterations in mitochondrial function likely also result in ER stress or vice versa; ER stress was
314 previously demonstrated in nephropathic cystinosis. Our study revealed increased ER wrapping of
315 mitochondria in CTNS$^{-/-}$ RPTECs. ER–mitochondria connection called mitochondria-ER associated
316 membranes (MAMs) occur when ER is stressed (65). MAMs mediate apoptosis, which is known to be
317 higher in nephropathic cystinosis. However, it's interesting to note that ATP6V0A1 overexpression did
318 not rescue ER-wrapping of mitochondria, or intracellular LDs in CTNS$^{-/-}$ RPTECs. LDs are known to be
319 induced by inflammation and ROS, and have been linked with neurodegenerative disorders (66). LDs
320 were never previously associated with cystinosis, thus further studies are needed to understand LD's role
321 in cystinosis.

322 Interestingly, similar to the overexpression of ATP6V0A1, ATX treatment rescued the cystinosis
323 phenotype in CTNS$^{-/-}$ RPTECs by – enhancing ATP6V0A1 expression, improving autophagosome
324 turnover, and improving mitochondrial structure and function. ATX also increased p53 levels, suggesting
325 a possible association between p53 and mitochondrial dysfunction. Previous studies demonstrated that
326 p53 overexpression led to an increase in superoxide and elevated $\Delta\Psi m$ (67) and some believe p53 may
327 act directly on mitochondria to release ROS and induce apoptosis (68). Further studies are needed to
328 clarify the role of ATX-induced p53 expression and mitochondrial function in CTNS$^{-/-}$ RPTECs. The
329 novel findings of this study are ATP6V0A1's role in cystinosis pathology, and that ATX can rescue
330 cystinotic RPTECs potentially by upregulating ATP6V0A1, offering a potential novel therapeutic for
331 limiting renal injury in nephropathic cystinosis. Although this is only a pilot study, our finding that ATX
332 in-vitro can ameliorate cystinosis-associated dysfunctional pathways is of paramount importance and
333 requires further study in cystinotic animal models and in combination with cysteamine to clarify its utility
334 in clinical settings.

335 **METHODS**

336 **Study design and Samples:**

337 Human RPTECs and fibroblasts were isolated from 8 unique individuals with a biochemically, clinically
338 and genetically confirmed diagnosis of nephropathic cystinosis (provided by Dr. Gahl) (21, 23); in
339 addition, similar cell types, RPTEC (Cambrex Biosciences, East Rutherford, NJ) and fibroblast
340 (Coriell Cell Repositories, Camden, NJ) cell lines were commercially obtained as normal control cells.
341 The patient derived RPTECs has its limitations, which are highlighted in the discussion section. Both
342 normal RPTECs and fibroblasts were treated with cysteine dimethyl ester (CDME) to artificially load
343 lysosomes with cystine, as this method has been used previously as a disease model for cystine RPTEC
344 loading, though it is unclear how accurate this model is for functional analysis of molecular changes in
345 cystinosis patient derived RPTECs (63, 69). In addition, we utilized an human immortalized (HuIm)
346 RPTEC line (Clone TH1, passage 8, Cat No. ECH001, Kerafast, Boston, MA), as control, and used
347 CRISPR-Cas9 to generate a $CTNS^{-/-}$ knock out HuIm RPTECs that was then structurally and functionally
348 characterized to evaluate it as an in vitro model system to study human cystinosis RPTEC injury. This
349 purchased HuIm RPTECs are derived from primary human renal proximal tubule epithelial cells
350 (RPTECs) immortalized by two lentiviral vectors carrying the human telomerase and the SV40 T antigen.
351 Details of the study design and its findings are shown in **Figure 1**.

352

353 All RPTECs were cultured in renal epithelial growth medium (REGM) (Lonza, Bend, OR); fibroblast
354 cells were cultured in Minimum Essential Media (MEM) with Earl's salts, supplemented with 15% FBS,
355 2mM L- glutamine, 2X conc. of non-essential AA, 100 µg/ml Penicillin, 100 U/ml Streptomycin and
356 0.5 µg/ml Fungizone (Invitrogen Corporation, Carlsbad, CA) at 37°C in a 5% CO2 atmosphere. The
357 medium was changed every alternate day, and cultured cells were harvested with 0.05% Trypsin/EDTA
358 (Lonza, Bend, OR) and passaged. All cells were cultured in a 95% air/5% CO2 Thermo Forma incubator
359 (Thermo Scientific, Waltham, MA) at 37°C. All the experiments were performed between passage
360 numbers 2-5. For CDME loading, cells were treated with 1mM CDME (Sigma-Aldrich, St. Louis, MO)

361 for 30 min. For ATX treatment, cells were pretreated with 10uM and 20uM ATX (Cat. No SML0982,
362 Millipore Sigma, Burlington, MA) for 48hr.
363
364 Since variation in genetic background and characteristics of patient and normal RPTECs can result in
365 experimental variations, independent of the *CTNS* mutation, immortalized healthy RPTEC cell lines
366 (Kerafast, Boston, MA) were used to generate isogenic $CTNS^{-/-}$ cell lines. CRISPR-Cas9
367 ribonucleoproteins (crRNPs) were synthesized in vitro by the incubation of CTNS-specific guide RNA,
368 trans-activating crRNA (tracrRNA), and Cas9 protein (Dharmacon, Lafayette, CO). These preformed
369 complexes were then delivered to immortalized RPTECs by nucleofection for editing. We used benchling
370 to design the guide RNA to specifically cut at exon 3 (70). Though this is not a known cystinosis-causing
371 mutation but such a knockout causes complete inactivation of cystinosin, which is the common output of
372 all the known mutations associated with nephropathic cystinosis. Since efficiency of gene-knockout
373 varies from one cell to other, we sorted single cells by FACS, amplified over the cut-site using touch-
374 down PCR amplification, and then submitted the PCR products for Sanger sequencing using both the
375 forward and reverse TIDE oligos originally used for amplification. Once the chromatograms were
376 returned, we chose to populate and use cells with at least 95% allelic editing, which provided a rough
377 estimate of knock-out percentages (**Figure 3**).
378
379 To detect the phenotype of these newly developed $CTNS^{-/-}$ cell lines, we performed a functional assay
380 measuring intracellular cystine levels using an HPLC-MS/MS method (UCSD Biochemical Genetics, San
381 Diego) and high levels of intracellular cystine in the generated $CTNS^{-/-}$ cell line compared to control cells.
382 The level of intracellular cystine accumulation in $CTNS^{-/-}$ cell lines were comparable to cystine levels in
383 cystinosis patients (**Figure 3C**).
384
385 **RNA Isolation**
386

387 Cells were grown until 70-80% confluence and processed for total RNA extraction using RNeasy Midi
388 Kit® (Qiagen Inc., Germantown, MD). Total RNA concentration was measured by NanoDrop® ND-1000
389 (NanoDrop Technologies, Wilmington, DE) and the integrity of the extracted total RNA was assessed
390 with the Agilent 2100 Bioanalyzer using RNA Nano Chips (Agilent Technologies, Santa Clara, CA).
391 Total RNA was stored at -80°C until preparation for the microarray experiments.
392
393 **Microarray Experiments to Characterize RPTEC and Fibroblast Transcriptional Profiles in**
394 **Nephropathic Cystinosis**
395
396 Hybridization of samples was conducted on Agilent Whole Human Genome 4×44-k 60-mer
397 oligonucleotide arrays (G4112F, Agilent Technologies, Santa Clara, CA), using 150ng of total RNA as
398 template/sample. The arrays were scanned on an Agilent scanner and further processed using Agilent
399 Feature Extraction Software (Agilent Technologies, Santa Clara, CA).
400
401 **Lysosomal Fractionation**
402
403 Lysosomal fractions were isolated from cultured cells by density gradient separation using the lysosome
404 enrichment kit (Pierce Biotechnology, Waltham, MA) for both tissue and cultured cells, following the
405 protocol provided by Pierce. Fraction purity was assessed by western blot using lysosome-specific
406 antibody against LAMP2.
407
408 **Western Blot**
409
410 Whole cells and lysosomal extracts were prepared, and an equal amount of protein (15ug) was subjected
411 to SDS-PAGE. All primary antibody incubations were done in PBS supplemented with 0.1% Tween-20

412 (vol/vol) and 5% milk (wt/vol) overnight followed by washing with PBS-Tween (PBS supplemented with
413 0.1% Tween). The primary antibodies used were: ATP6V0A1 (Cat. No. 109002, Synaptic Systems,
414 Goettingen, Germany), LAMP2 (Cat. No. sc18822, Santa Cruz Biotechnology, Santa Cruz, CA), LC3B
415 (Cat. No. 3868, Cell Signaling, Danvers, MA), phospho-p70 S6 Kinase (Thr389) (Cat. No. MAB S82,
416 Millipore Sigma, Burlington, MA) GAPDH (Cat. No. 97166S, Cell Signaling, Danvers, MA), beta-
417 tubulin (Cat. No. 2128S, Cell Signaling, Danvers, MA), and p53 (Cat. No. A5761, Abclonal, Woburn,
418 MA). The Peroxidase-conjugated secondary antibodies were diluted 1:2000 in PBS-Tween, incubated
419 with the blot for a minimum of 1 hour at room temperature, and then washed with PBS-Tween and
420 developed using Amersham ECL Plus Detection Reagent (RPN2124, Millipore Sigma, Burlington, MA).
421 Loading levels were normalized using 1:2000 anti-GAPDH or beta-tubulin and anti-LAMP2 Abs. Band
422 quantification was performed using the ImageLab software (National Institutes of Health).

423

424 **Measurement of pH**

425 The conversion of non-fluorescent 2',7'-bis-(2-carboxyethyl)-5-(and-6)-carboxyfluorescein
426 acetoxymethyl ester (BCECF AM) (Invitrogen, Waltham, MA) into a pH sensitive fluorescent indicator
427 by the intracellular esterase was used to measure the pH within the cell. We seeded a fixed number of cells
428 in a clear-bottom black 96-well plate, incubated overnight in a CO_2 incubator, and then
429 measured pH. The fluorescence ratio was acquired using the SpectraMax iD3 plate reader (Molecular
430 Devices, San Jose, CA) (excitation = 490, 440 nm; emission = 535 nm). The ratio of BCECF fluorescence
431 at 490/440 nm is a function of pH.

432 **Measurement of mitochondrial oxygen consumption rate**

433

434 The Agilent Seahorse XFe analyzer allows for real-time measurements of cellular metabolic function in
435 cultured cells. The oxygen consumption rate (OCR) was measured by the extracellular flux analyzer XF24

436 (Seahorse Bioscience, Santa Clara, CA) following optimization of cell number per well. RPTECs were
437 plated at 4 x 10^5 cells/well in a Seahorse 24-well V7 microplate (Seahorse Bioscience, Santa Clara, CA)
438 and cultured in complete renal epithelial growth medium for 16-18 h in a 5% CO_2 incubator at 37°C. Prior
439 to the assay, the cells were washed and incubated with assay media (Agilent Technologies, Santa Clara,
440 CA) supplemented with 1 mM glucose (Agilent Technologies, Santa Clara, CA), 1 mM pyruvate (Agilent
441 Technologies), and 2 mM glutamine (Agilent Technologies, Santa Clara, CA) at 37°C without CO_2 for 45
442 min. Mitochondrial function was measured using Seahorse XF Cell Mito Stress test (Agilent
443 Technologies, Santa Clara, CA). Mitochondrial complex inhibitors (oligomycin, FCCP, rotenone and
444 antimycin A) were freshly prepared in XF assay media prior to each experiment.
445 OCR following serial injection of various probes was used as an indicator of mitochondrial
446 function. Oligomycin, an ATP synthase inhibitor, was utilized as a probe for ATP-linked oxygen
447 consumption; carbonyl cyanide-4-(trifluoromethoxy)phenylhydrazone (FCCP), an oxidative
448 phosphorylation uncoupling agent, was used to induce maximum oxygen consumption and the resultant
449 OCR was used to calculate spare respiratory capacity. A mixture of rotenone and antimycin-A inhibited
450 complex I and complex III was used to result in complete inhibition of mitochondrial respiration and
451 determination of non-mitochondrial oxygen consumption. We compared the pattern observed after
452 injection of each inhibitor in cystinotic RPTECs.
453
454 **Overexpression of ATP6V0A1**
455
456 For ATP6V0A1 overexpression, Myc-DDK-tagged ATP6V0A1 expression plasmid (RC226206,
457 Origene, Rockville, MD) for ATP6V0A1 induction and pCMV6-Entry, mammalian vector with C-
458 terminal Myc-DDK Tag (PS100001, Origene, Rockville, MD) for control were used. Briefly, 3×10^5
459 $CTNS^{-/-}$ and control RPTECs were seeded in six-well plates and incubated for 24 hours prior to
460 transfection. TurboFectin 8.0 Transfection Reagent (F81001, Origene, Rockville, MD) was used at a final

461 concentration of 4ug/ml for transduction. The overexpression of ATP6V0A1 was verified with western
462 blotting analysis.
463
464 **Confocal Microscopy**
465

466 For immunofluorescence, RPTECs were plated in 4-well Chamber Slide with removable wells
467 (ThermoFisher, Waltham, MA), fixed in 100% chilled methanol (5 minutes), permeabilized with PBS
468 containing 0.25% Triton X-100 (10 minutes), and washed three times in PBS. Cells were incubated in
469 10% normal goat serum blocking solution (Invitrogen, Waltham, MA) for 1 hour followed by overnight
470 primary antibody incubation in a 4°C humidified chamber. For co-immunostaining, we added both
471 primary antibodies raised in different host species, at the same time. Next day, slides were washed three
472 times in PBS and followed by secondary antibody incubation in 1% BSA for 1 h at room temperature in
473 the dark. After washing with PBS, the cells were counterstained with DAPI for 5 min and then washed.
474 The 1.5mm thick coverslip was then mounted with a drop of ProLong Glass Antifade Mountant
475 (ThermoFisher, Waltham, MA). Primary antibodies used were: LAMP2 (Santa Cruz Biotechnology,
476 Santa Cruz, CA), ATP6V1B2 (Abcam, Cambridge, United Kingdom), ATP6V0A1 (Synaptic Systems,
477 Goettingen, Germany), LC3B (Cell Signaling Technology, Danvers, MA), phosphor-p70S6 Kinase
478 (Thr398) (Millipore Sigma-Aldrich, St. Louis, MO). Secondary antibodies, donkey anti-Rabbit IgG Alexa
479 Fluor 488 and goat anti-Mouse IgG Alexa Fluor 555 (ThermoFisher, Waltham, MA) were used to detect
480 bound primary antibody. Slides were viewed using a Leica SP5 Confocal Laser Scanning Microscope,
481 and the images were analyzed by Leica Confocal software.

482
483 **Transmission Electron Microscopy (TEM)**
484

485 3×10^5 RPTECs were seeded in each well of a six well plate and maintained for 24 h. On the day of the
486 experiment, fresh 2% glutaraldehyde was generated from an 8% stock glutaraldehyde in complete REGM
487 culture media and was added to each well so that cells were fully covered with fixative. After 15 min, the
488 fixed cells were scrapped gently and transferred to a microcentrifuge tube. The samples were centrifuged
489 and the supernatant was discarded followed by the quick addition of 1ml fresh fixative (2%
490 glutaraldehyde in 0.1M Cacodylate buffer pH 7.2). At this stage, the cells were stored at 4°C and were
491 then handed over to the Electron Microscope Laboratory (EML) imaging core at the University of
492 California, Berkeley for sectioning and imaging. Sections were cut at 80 nm, stained with lead citrate and
493 uranyl acetate, and examined under an FEI Tecnai12 electron microscope (FEI). The electron micrographs
494 obtained from multiple distinct low-powered fields were used to count the number of mitochondria and
495 autophagic vacuoles per cell in at least eight different view fields for each cell culture sample, and the
496 average number of mitochondria or autophagic vacuole per cell culture was calculated.
497
498 **Mitochondrial Membrane Potential Assay**
499
500 The mitochondrial membrane potential ($\Delta\Psi m$) was measured with the JC-1 mitochondrial membrane
501 potential assay kit (ab113580, Abcam, Cambridge, United Kingdom) according to manufacturer's
502 instructions. Briefly, RPTEC were seeded at 12,000 cells/well and allowed to adhere overnight in a black
503 clear-bottom 96 well plate. Cells were treated with or without 10 or 20uM ATX for 48hr and then washed
504 once with 1X dilution buffer prior to incubation with 20uM JC-1 dye for 10 min at 37°C. Following
505 incubation, cells were washed twice with 1X dilution buffer and fluorescence intensity was determined
506 for red aggregates (excitation = 535 nm)/emission = 590 nm) and green monomers (excitation =
507 475 nm/emission = 530 nm) with the SpectraMax iD3 plate reader (Molecular Devices, San Jose, CA).
508 The ratio of JC-1 aggregates (590nm) to JC-1 monomers (530nm) was calculated. A decrease in
509 aggregate fluorescent count is indicative of depolarization whereas an increase is indicative of
510 hyperpolarization.

511

512 **Mitochondrial ROS Production and Cell Viability**

513 Mitochondrial ROS production was assessed using MitoSox Red superoxide indicator (ThermoFisher,
514 Waltham, MA). Briefly, cells plated at 10,000 cells/well in 96-well plates were washed with Hanks
515 balanced salt solution (HBSS) (ThermoFisher, Waltham, MA) and treated with 5uM MitoSOX for 15 min
516 at 37C and 5% CO2, protected from light. After staining, cells were washed twice with HBSS to remove
517 background fluorescence. Fluorescence was read (excitation= 510nm, emission= 580nm) with the
518 SpectraMax iD3 plate reader (Molecular Devices, San Jose, CA). Following MitoSox assay, cells were
519 washed with HBSS and WST-1 (Abcam, Cambridge, United Kingdom) was added to plate and incubated
520 for 30min at 37°C and 5% CO_2 to measure the cell viability. Absorbance was read at 440nm to assess cell
521 viability. Mitochondrial ROS production was normalized to cell viability.

522 **Statistics**

523 Agilent array data were processed and normalized using LOWESS in Gene Spring GX7.3 (Agilent
524 Technologies). The LOWESS normalized data were further analyzed using significance analysis of
525 microarrays (SAM) for two-class unpaired data to detect expression differences based on q-values
526 (<5%)(71). The input for SAM was gene expression measurements from a set of microarray experiments,
527 as well as a response variable from each experiment. SAM used simple median centering of the arrays is
528 an unbiased statistical technique for finding significant genes in a set of microarray experiments. SAM
529 uses repeated permutations of the data to determine whether the expression of each gene is significantly
530 related to the response. Significance levels were set at a q-value of 5%. We used a cutoff of the absolute
531 value of $\log_2$ red channel/green channel >0.5. Data were analyzed using GraphPad Prism software. P-
532 values were calculated using Student's t-test or One-way ANOVA and Tukey' test. Results were
533 expressed as mean ± SD (number of experiments) and considered to be statistically significant when $P <$
534 0.05.

535 **MATERIALS AVAILABILITY**

536 We did not use human or animal models but we have used human cells for this study. Cystinosis RPTE
537 and fibroblast cells are gifts from Dr. Gahl and Dr. Racusen. In addition, the cell lines are commercially
538 purchased. CRISPR-edited renal cell line is available in Sarwal Lab. Please email:
539 Minnie.sarwal@ucsf.edu or Swastika.sur@ucsf.edu. The study was controlled by institutional review
540 board approvals from the National Institute of Health, Stanford University and the Regents, University of
541 California.

542 **DATA AVAILABILITY**

543 The transcriptomic data was submitted to GEO. The GEO Accession number is GSE190500.

544 **AUTHOR CONTRIBUTIONS**

545 S.S. and M.S. designed the study; S.S., M.K. and P.S. carried out the experiments; S.S., M.K., S.P., M.S.
546 analyzed the data; S.S. and M.K. made the figures; S.S., M.K., T.K.S., M.S. drafted and revised the paper;
547 all authors approved the final version of the manuscript.

548 **ACKNOWLEDGMENTS**

549 We thank Dr. William Gahl and Dr. Lorraine Racusen for the generous gift of cystinosis RPTE and
550 fibroblast cells and Reena Zalpuri at the University of California Berkeley Electron Microscope
551 Laboratory for advice and assistance in electron microscopy sample preparation and data collection. In
552 addition, we would also like to thank Jon Gangoiti at the UCSD Biochemical Genetics Laboratory for
553 advice on sample preparations and performing HPLC-MS/MS method to measure intracellular cystine
554 levels. This work was supported by grants from the Health Research Board, Ireland and The Cystinosis
555 Foundation, Ireland.

556 **FIGURES**

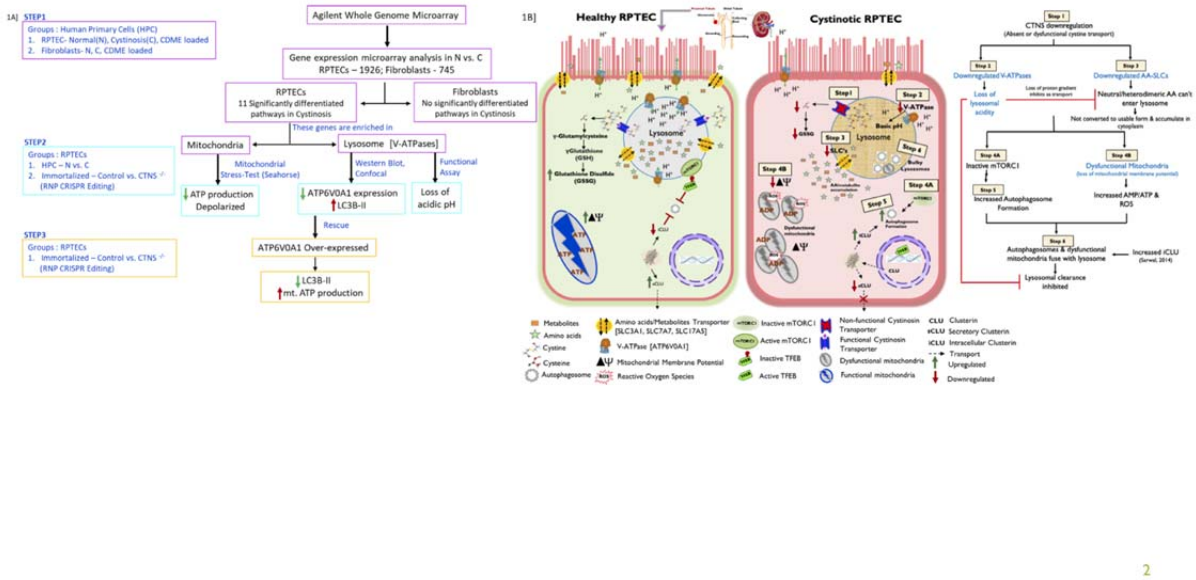

557 **Fig. 1: Overall study design, workflow, and schematic overview**. (**A**) Transcriptome profiling with
558 gene microarray performed on cystinotic, normal, and CDME-treated RPTECs and fibroblasts (Step 1).
559 Bioinformatic analysis allowed the identification of genes that are differentially regulated in cystinosis
560 versus normal in both the cell types. Pathway analysis was performed with all the significantly regulated
561 genes, and 11 pathways were found to be significantly affected in cystinotic RPTECs. Most of these
562 pathways and the genes in these pathways are crucial for lysosomal acidic pH and mitochondrial ATP
563 production. Dysfunctional mitochondria and compromised lysosomal pH were validated in step 2. Our
564 CRISPR-mediated CTNS$^{-/-}$ immortalized renal cell line mimicked cystinosis patient primary cells isolated
565 from their urine. Further, we rescued (Step 3) the disease phenotype of the cell by over-expressing
566 ATP6V0A1, the most significantly downregulated gene among other V-ATPases. RNP,

567 Ribonucleoprotein; V-ATPase, vacuolar ATPase; RPTEC, renal proximal tubular epithelial cells. (**B**) A
568 schematic overview of normal and cystinotic RPTECs. We previously showed that loss of function of
569 cystinosin in cystinotic cells inactivates the mTORC pathway, and induces autophagy, mitophagy, and
570 clusterin protein expression. In this study, we show that downregulation of CTNS gene also
571 downregulates V-ATPase expression resulting in the loss of lysosomal acidity (pH). The basic lysosomal
572 pH thus blocks its clearance after autophagosome-lysosome fusion. Inhibited autophagy flux due to
573 lysosomal acidity loss may explain why cystinotic cells have increased LC3B-II expression. Loss of
574 acidic lysosomal pH also impairs proton-dependent import of amino acids and other metabolites (noted in
575 our microarray data) into the lysosome lumen, and inhibits conversion of these imported large
576 heterodimeric amino acids into usable form. This increases the presence of metabolites in the cytoplasm
577 that may compromise mitochondrial function and increase ROS production through an unspecified
578 mechanism.
579
580
581
582
583
584

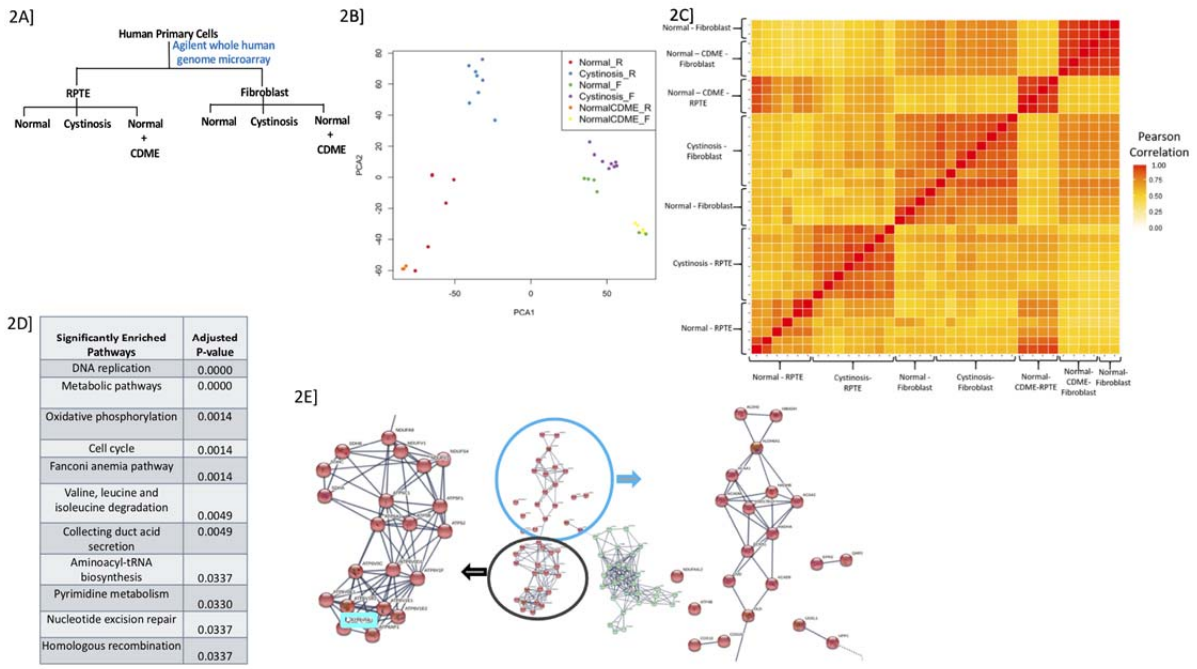

Significantly Enriched Pathways	Adjusted P-value
DNA replication	0.0000
Metabolic pathways	0.0000
Oxidative phosphorylation	0.0014
Cell cycle	0.0014
Fanconi anemia pathway	0.0014
Valine, leucine and isoleucine degradation	0.0049
Collecting duct acid secretion	0.0049
Aminoacyl-tRNA biosynthesis	0.0337
Pyrimidine metabolism	0.0330
Nucleotide excision repair	0.0337
Homologous recombination	0.0337

Fig. 2: Microarray study design and transcriptional changes for cystinotic, normal, and CDME-treated RPTECs or fibroblasts. (**A**) Study design: Two types of cells were used- RPTECs and fibroblasts. For each cell type there were three groups – normal that serves as control, cystinotic, and CDME-treated cells. (**B**) Microarray data from both cell types are represented as a correlation heatmap. Cystinotic RPTECs showed markedly different expression profiles from both the normal and CDME loaded normal RPTEC, which was more similar to normal than diseased. Gene expression patterns in normal, cystinotic, and CDME-treated fibroblasts were found to be similar to each other. (**C**) PCA plot further highlights the unique injury mediated gene profile in cystinotic RPTEC versus normal. Gene expression patterns of cystinotic RPTECs and fibroblasts were found to have no commonality, with cystinostic fibroblasts similar to normal. Gene expression patterns in cystinotic RPTECs are distinct and negatively correlated with normal RPTECs. Whereas gene expression in normal

597 RPTECs laden with CDME are similar to the normal rather than disease phenotype, and hence have a
598 positive correlation with each other. (**D**) Pathway analysis was performed with all the significantly
599 regulated genes, and 11 pathways were found to be significantly affected in cystinotic RPTECs. (**E**)
600 Using K-mean clustering on the genes in these significantly enriched pathways, we identified 2 distinct
601 clusters. One, is enriched in nucleus-encoded mitochondrial genes, and the other is enriched in v-ATPases
602 family, which are crucial for lysosomes and kidney tubular acid secretion. ATP6V0A1, the topmost v-
603 ATPase in our cystinotic transcriptome dataset is highlighted in cyan.
604
605
606
607
608
609
610
611
612
613
614
615
616
617
618
619
620
621
622

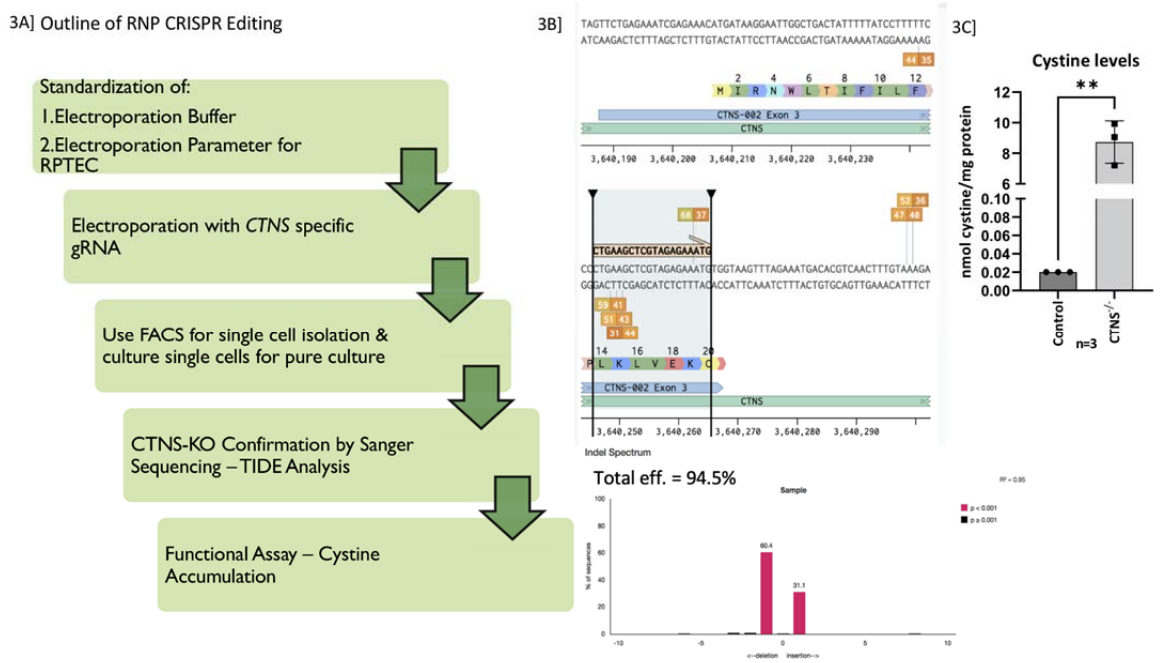

Fig. 3: **Experimental overview for the development of immortalized *CTNS*$^{-/-}$ RPTECs using CRISPR-Cas9 RNPs.** (**A**) Briefly, The CTNS gene is located on chromosome 17p13.3 and consists of 12 exons, of which the first 2 are non-coding. Therefore, our guide RNA was targeted towards exon 3 to completely knockout the functional *CTNS* gene. CRISPR-Cas9 ribonucleoproteins (crRNPs) were synthesized in vitro to knockout CTNS gene and delivered to immortalized RPTECs by nucleofection. These cells were expanded for molecular validation of gene editing and downstream functional assays. (**B**) The guide RNA target sequence and associated PAM are highlighted on the right. The TIDE output calculating percent indels from chromatograms is depicted below. (**C**) Validation of CTNS knockout in immortalized RPTEC. Increased intracellular accumulation of cystine is shown by HPLC-MS/MS method in control and *CTNS*$^{-/-}$ RPTECs.

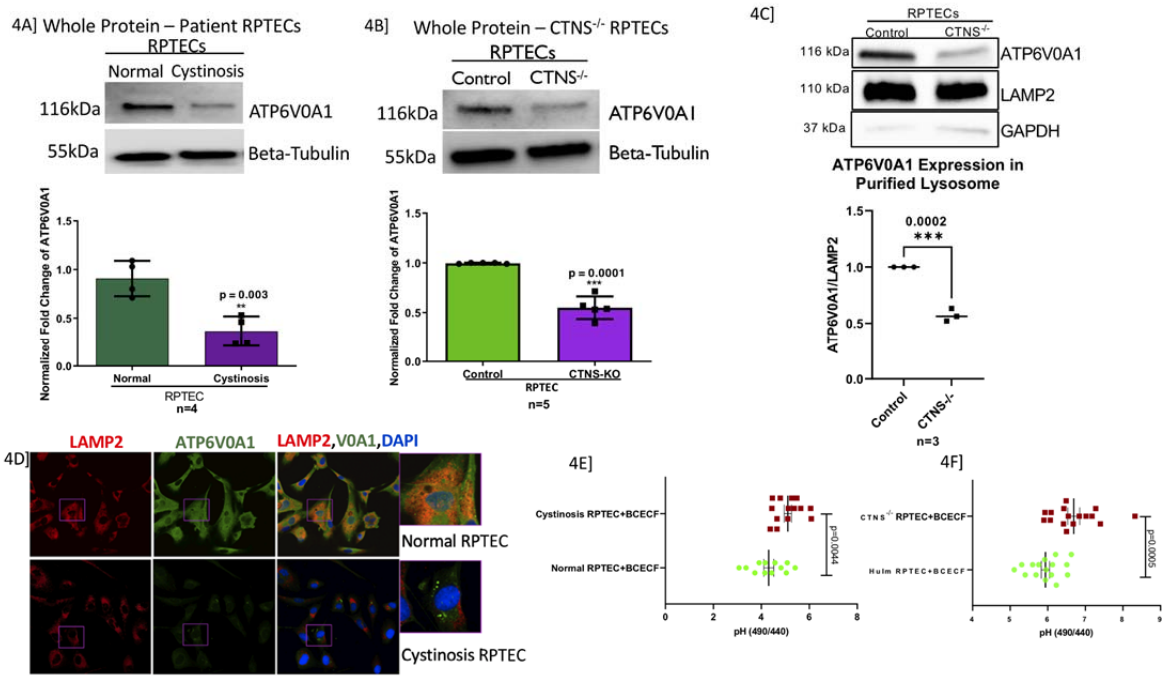

634

635 **Fig. 4**: **Vacuolar-ATPase, ATP6V0A1, is downregulated in both, cystinotic and *CTNS*$^{-/-}$ RPTECs,**
636 **confirming that our *in vitro* model behaves similarly to primary cystinotic renal cells.** This highlights
637 that in addition to the loss of lysosomal cystinosin there are also other key biological changes in the
638 lysosomes in nephropathic cystinosis. (**A-B**) Immunoblot analysis of the expression of ATP6V0A1 in
639 cystinotic (p=0.003) and *CTNS*$^{-/-}$ RPTECs (p=0.0001) with their respective controls. (**C**) Immunoblot
640 showing high expression of lysosome marker LAMP2 and decreased GAPDH expression, collectively
641 represents successful isolation of lysosomes from RPTECs. (**D**) Immunoblot analysis of the expression of
642 ATP6V0A1 in lysosomal fraction isolated from control (HuIm RPTEC) and *CTNS*$^{-/-}$ (HuIm) RPTECs.
643 Results are represented as mean ± SD. The statistically significant differences between the two groups are
644 indicated in the figure. Student's t-test (* $P \leq 0.05$; ** $P \leq 0.01$; *** $P \leq 0.001$). (**E**) Immunofluorescence and
645 confocal microscopy showing endogenous LAMP1 and ATP6V0A1 distribution in normal (control) and

646 cystinotic (diseased) RPTECs. Colocalization of ATP6V0A1 and LAMP2 is shown in the right panel.
647 Results are representative of at least 3 separate experiments. Cystinotic and *CTNS*$^{-/-}$ RPTECs have an
648 intracellular basic pH compared to their respective controls. Cells were stained with BCECF-AM and
649 measured with a microplate fluorimeter in triplicate wells. The pH-dependent spectral shifts exhibited by
650 BCECF allow calibration of the pH response in terms of the ratio of fluorescence intensities measured at
651 two different excitation wavelengths (490, 440 nm). (**F**) RPTECs isolated from cystinosis patient urine
652 had a more basic pH than normal individuals ((p=0.004). (G) Similarly to the primary cells, our in vitro
653 cellular model, *CTNS*$^{-/-}$ RPTEC, also had a more basic pH than control p=0.0005. The unpaired *t*-test
654 indicated significant differences between control and diseased cells. Data are representative of three
655 biological replicates. Values represent mean ±SD for three independent experiments.
656
657
658
659
660
661
662

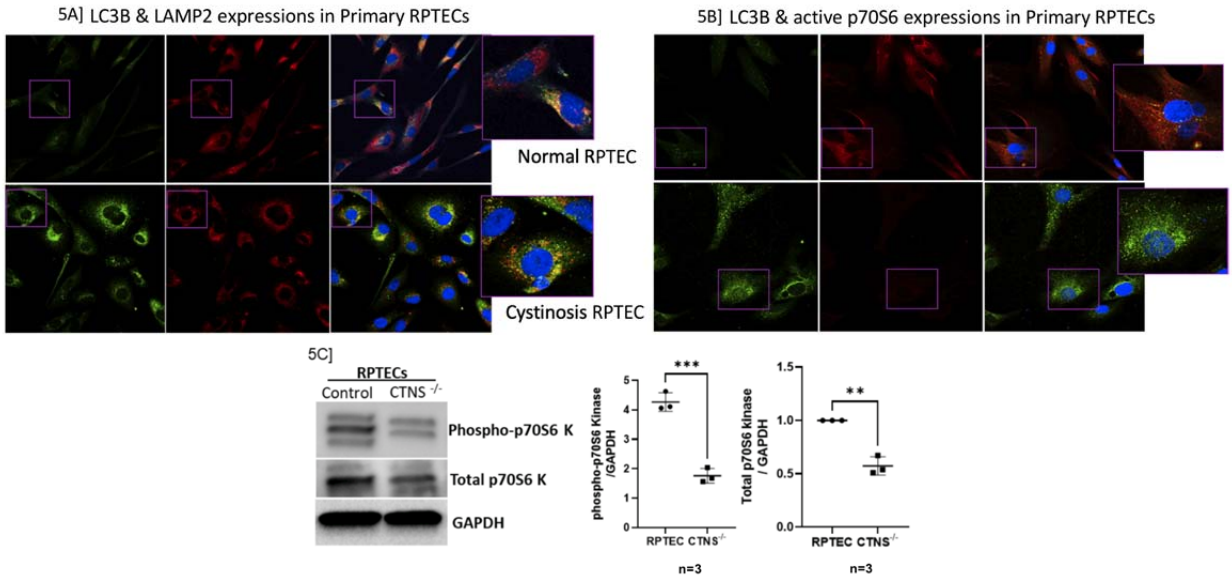

Fig. 5: Increased immunopositivity to LC3B-II, or autophagy, and decreased immunopositivity to phospho-p70S6 kinase, or mTORC1 activity. (**A**) Immunofluorescence and confocal microscopy showing endogenous LC3B and LAMP2 distribution in normal and cystinotic RPTECs. Colocalization of LC3B and LAMP2 is shown in the right panel. (**B**) Immunofluorescence and confocal microscopy showing endogenous LC3B and phospho-p70S6 kinase (marker of mTOR activity) distribution in normal and cystinotic RPTECs. Since mTORC1 plays a central role in cell growth, proliferation, survival, and autophagy inhibition via AMPK, the presence of lower activity of mTORC1 in cystinosis supports the observations of increased cell death and autophagy as shown by increased LC3B puncta. Colocalization of LC3B and phosphor-p70S6 kinase is shown in the right panel. Results are representative of at least 3 separate experiments (biological replicates). (C) Immunoblots showing reduced immunopositivity towards phosphorylated-p70S6 kinase protein, a direct downstream substrate

675 of mTORC1 and common marker of mTOR activity. Since there is a change in total p70S6K expression
676 in with and without the CTNS, we normalized both, the phosphorylated and total protein, to GAPDH.
677
678
679
680
681
682
683
684
685
686
687

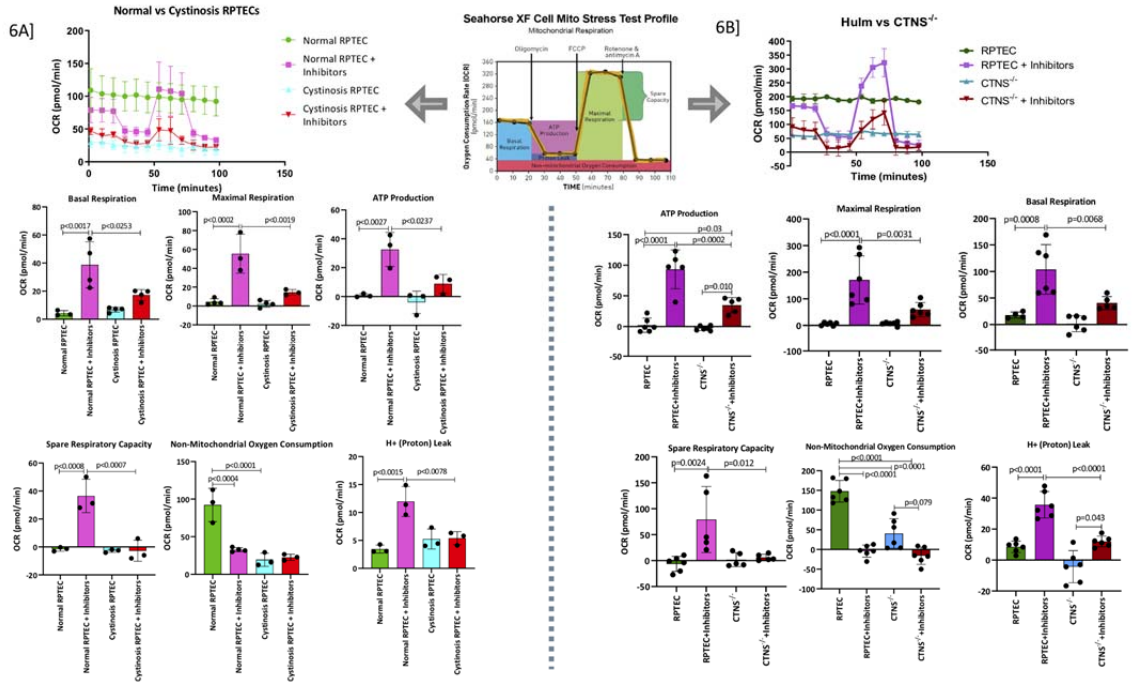

688

689 **Fig. 6: The Agilent Seahorse Mitochondria Stress Test detected mitochondrial defects in primary**
690 **cystinotic and *CTNS*$^{-/-}$ RPTECs compared to their respective controls.** Top Center) XF Cell Mito
691 Stress Test assay design and standard output parameters. (**A**) XF Cell Mito Stress Test shows that primary
692 cystinotic RPTECs with specific inhibitors display diminished basal and maximal respiration, ATP
693 production, spare respiratory capacity, non-mitochondrial oxygen consumption, and proton leak
694 compared with its control (normal RPTEC). (**B**) Similar to the primary diseased cells, the *CTNS*$^{-/-}$ also
695 demonstrated diminished mitochondrial activity. Both cystinotic and CTNS$^{-/-}$ RPTECs exhibited similar
696 patterns of compromised mitochondrial function, with significantly (Normal vs. Cystinosis: $p<0.025$,
697 $p<0.0019$, $p<0.023$; human immortalized RPTEC (HuIm) vs. CTNS$^{-/-}$: $p=0.006$, $p=0.001$, $p=0.0002$,
698 respectively) decreased basal and maximal respiration and ATP production compared to controls. The
699 OCR linked to proton leak and cells spare respiratory capacity was significantly (Normal vs. Cystinosis:

700 $p<0.007$, $p<0.0007$; HuIm vs. $CTNS^{-/-}$: $p<0.0001$, $p=0.002$ respectively) lost in cystinotic cells. Non-
701 mitochondrial oxygen consumption did not significantly change in cystinotic or $CTNS^{-/-}$ RPTECs. There
702 was a substantial (Normal vs. Cystinosis: $p<0.007$; HuIm vs. $CTNS^{-/-}$: $p<0.0001$) increase in OCR linked
703 to proton leak. Values represent mean ± SD for three independent experiments (* $P \leq 0.05$; ** $P \leq 0.01$;
704 *** $P \leq 0.001$). OCR, oxygen consumption rate.
705
706
707
708
709
710
711
712
713
714
715
716
717
718
719
720
721
722
723
724

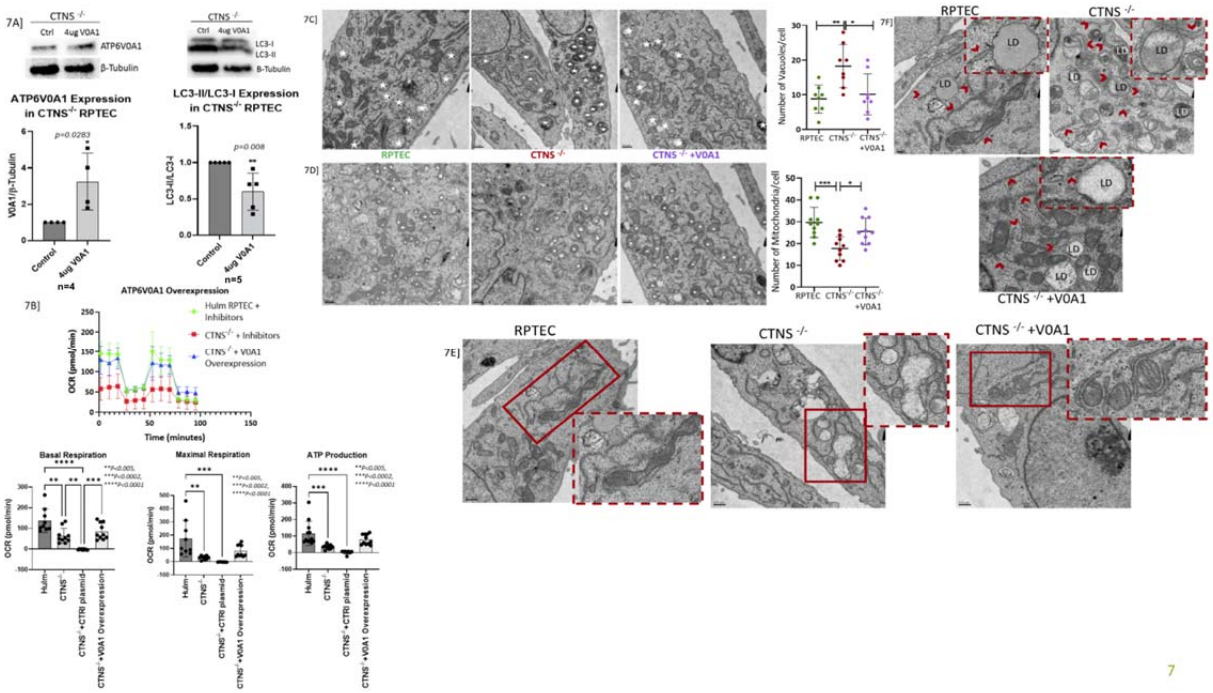

725

726 **Fig. 7: Overexpression of ATP6V0A1, by transfecting the CTNS$^{-/-}$ RPTECs with a Myc-DDK-**

727 **tagged human ATP6V0A1-plasmid, partially rescued the disease cell phenotype.** (**A**) Immunoblot

728 showing successful overexpression of ATP6V0A1 protein in the CTNS$^{-/-}$ cells. Values represent mean ±

729 SD for three independent experiments (* $P \leq 0.05$; ** $P \leq 0.01$; *** $P \leq 0.001$). Overexpression of

730 ATP6V0A1 significantly reduced the LC3-II protein expression. Values represent mean ± SD for three

731 independent experiments (* $P \leq 0.05$; ** $P \leq 0.01$; *** $P \leq 0.001$). (**B**) The XF Cell Mito Stress Test shows

732 that overexpression of ATP6V0A1 in CTNS$^{-/-}$ cells significantly improved basal respiration, and increased

733 maximal respiration and ATP production. Overall, ATP6V0A1 overexpression in CTNS$^{-/-}$ cells most

734 closely resemble the normal human immortalized (HuIm) RPTECs compared to CTNS$^{-/-}$ or CTNS$^{-/-}$ with

735 control plasmid. Values represent mean ± SD for three independent experiments (* $P \leq 0.05$; ** $P \leq 0.01$;

736 ***$P \leq 0.001$). Electron microscopic evaluation of CTNS$^{-/-}$ RPTECs, and its partial recovery by
737 overexpressing ATP6V0A1. (**C**) TEM of control, CTNS$^{-/-}$, and ATP6V0A1 overexpressed CTNS$^{-/-}$
738 (CTNS$^{-/-}$ +V0A1) RPTECs at low magnification. Asterisks indicate autophagic vacuoles (AV). Number of
739 AV per cell from 8 different sections of each sample was counted and depicted as a bar graph. Significant
740 increase in AV (p=0.006) is observed in CTNS$^{-/-}$ compared to that of RPTECs and CTNS$^{-/-}$ +V0A1
741 groups. (**D**) TEM of control, CTNS$^{-/-}$, and CTNS$^{-/-}$ +V0A1 RPTECs at low magnification. Asterisks
742 indicate mitochondria. Number of mitochondria per cell from 8 different sections of each sample was
743 counted and depicted as a bar graph. Significant decrease (p=0.0005) in mitochondria is observed in
744 CTNS$^{-/-}$ compared to that of RPTECs and CTNS$^{-/-}$ +V0A1 groups. Both figures A and B indicates rescue
745 of the diseased phenotype by the overexpression of ATP6V0A1 (p=0.019; p=0.02, respectively). (**E**)
746 Structurally abnormal ER-wrapped mitochondria with lesser cristae was observed in CTNS$^{-/-}$ compared to
747 that of RPTECs. Though, structurally normal mitochondria with cristae was observed in CTNS$^{-/-}$ +V0A1
748 group, but majority of the mitochondria are wrapped by ER. Scale = 0.5um. (**F**) Intracellular LD was
749 observed in more number of cells in CTNS$^{-/-}$ and CTNS$^{-/-}$ +V0A1 samples than control RPTECs. LDs
750 have a unique structure, which is delimited by a monolayer of phospholipids differing from the classical
751 bilayer structural organization. Arrows indicate endoplasmic reticulum (ER). Scale = 0.2um.
752
753
754
755
756
757
758
759
760
761

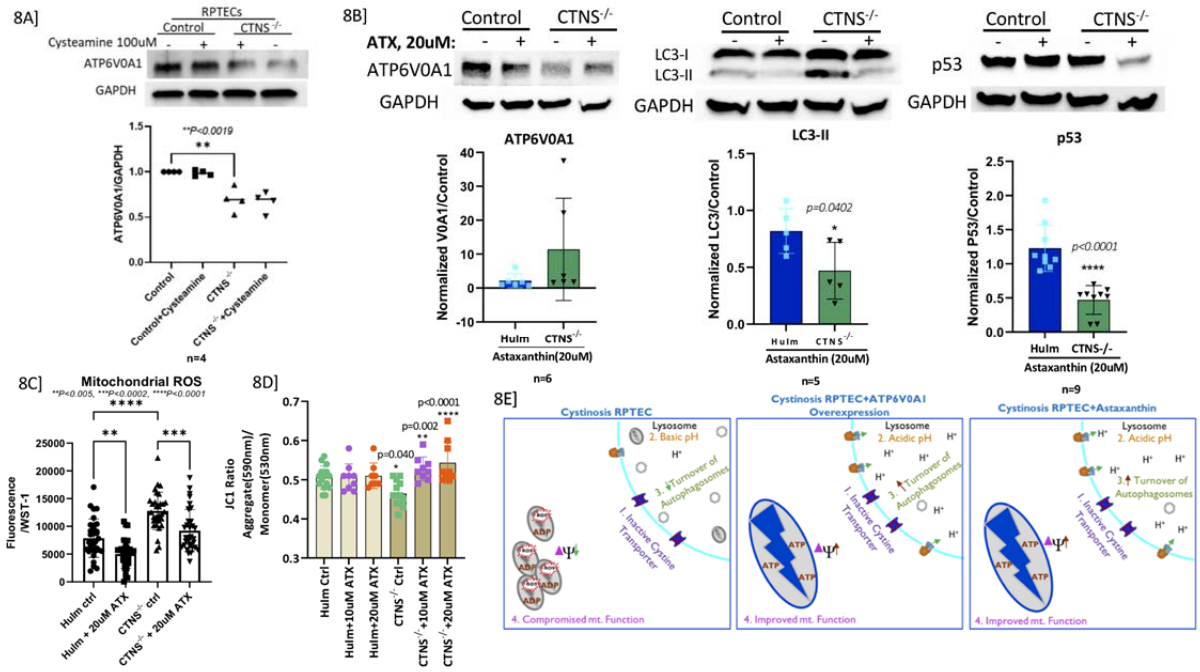

Fig. 8: ATX improved autophago-lysosomal turnover and mitochondrial health in cystinosis RPTEC phenotype. (**A**) Immunoblot showing that 100uM of cysteamine treatment for 24 hours did not increase the expression of ATP6V0A1 in CTNS$^{-/-}$ RPTECs. ATX improved mitochondrial membrane potential (p=0.002, p<0.0001 at both 10uM and 20uM, respectively) in CTNS$^{-/-}$ as shown by the JC1 ratio. (**B**) Immunoblot showing ATX upregulates ATP6V0A1, reduced the LC3-II (p=0.04) and p53 (p<0.0001) protein expression. Values represent mean ± SD for three independent experiments (* $P \leq 0.05$; ** $P \leq 0.01$; *** $P \leq 0.001$). (**C**) ATX reduced (p=0.0002) mitochondrial ROS normalized to cell viability measured by WST-1. (**D**) ATX improved mitochondrial membrane potential (p=0.002, p<0.0001 at both 10uM and 20uM, respectively) in CTNS$^{-/-}$ as shown by the JC1 ratio. (**E**) Model of partial rescue from the cystinosis phenotype by ATP6V0A1 overexpression. In cystinotic cells, cystinosin downregulation (**step 1**)

774 accumulates cystine in the lysosome and also downregulates V-ATPase expression, resulting in loss of
775 lysosomal acidity (**step 2**). The basic lysosomal pH thus inhibits the autophagosome-lysosomal
776 degradation and import of amino acids and other metabolites into the vacuole lumen (**step 3**). The
777 increased presence of metabolites in the cytoplasm compromises mitochondrial function through an
778 unspecified mechanism (**step 4**). Overexpression of ATP6V0A1, the most significantly downregulated V-
779 ATPase in our data set, significantly increased autophagosome turnover by removing the buildup of LC3-
780 II and partially improved the mitochondrial function.
781
782
783
784
785
786
787
788
789
790
791
792
793
794
795
796
797
798

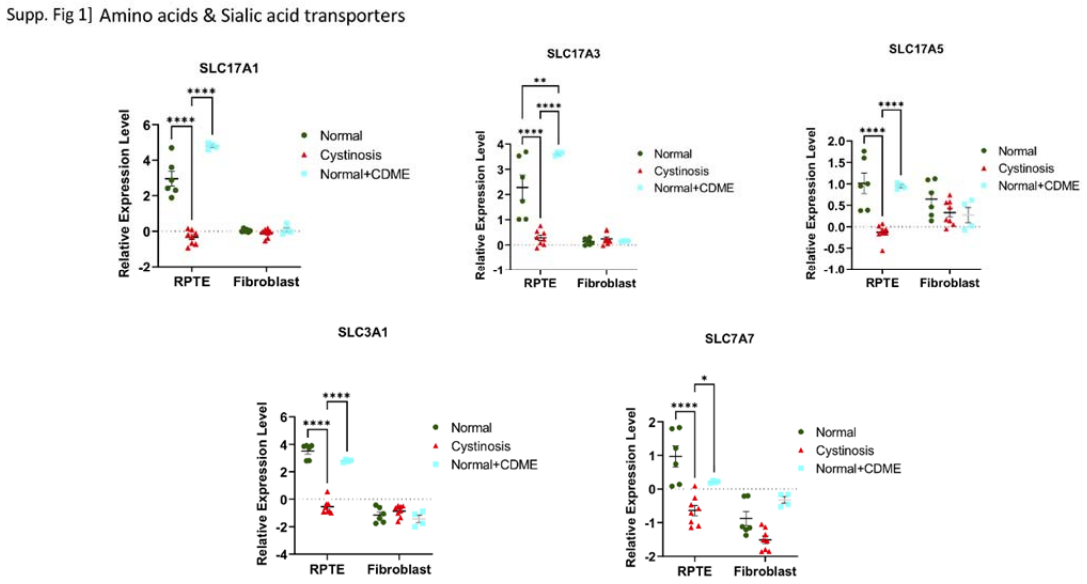

799 **Supplementary Material**

800

801 **Supplementary Figure 1: Amino Acids & Sialic Acid Transporters**. Microarray identified additional
802 transcriptional changes in amino acid and sialic acid transporters in cystinotic RPTEC. Significant
803 downregulation of SLC17A1, SLC17A3, SLC17A5, SLC3A1, and SLC7A7. (* $P \leq 0.05$; ** $P \leq 0.01$;
804 *** $P \leq 0.001$).

805

806

807

808

809 References

810

811 1. Ballabio A, Gieselmann V. Lysosomal disorders: from storage to cellular damage. Biochimica et

812 biophysica acta. 2009;1793(4):684-96.

813 2. Burton BK. Inborn errors of metabolism in infancy: a guide to diagnosis. Pediatrics.

814 1998;102(6):E69.

815 3. Fuller M, Meikle PJ, Hopwood JJ. Epidemiology of lysosomal storage diseases: an overview.

816 Fabry disease: perspectives from 5 years of FOS: Oxford PharmaGenesis; 2006.

817 4. Platt FM, Walkley SU. Lysosomal disorders of the brain. 2005.

818 5. Anikster Y, Shotelersuk V, Gahl WA. CTNS mutations in patients with cystinosis. Human

819 mutation. 1999;14(6):454-8.

820 6. Kalatzis V, Cherqui S, Antignac C, Gasnier B. Cystinosin, the protein defective in cystinosis, is a

821 H(+)-driven lysosomal cystine transporter. The EMBO journal. 2001;20(21):5940-9.

822 7. Town M, Jean G, Cherqui S, Attard M, Forestier L, Whitmore SA, et al. A novel gene encoding

823 an integral membrane protein is mutated in nephropathic cystinosis. Nature genetics. 1998;18(4):319-24.

824 8. Attard M, Jean G, Forestier L, Cherqui S, van't Hoff W, Broyer M, et al. Severity of phenotype in

825 cystinosis varies with mutations in the CTNS gene: predicted effect on the model of cystinosin. Human

826 molecular genetics. 1999;8(13):2507-14.

827 9. Anikster Y, Lucero C, Guo J, Huizing M, Shotelersuk V, Bernardini I, et al. Ocular

828 nonnephropathic cystinosis: clinical, biochemical, and molecular correlations. Pediatric research.

829 2000;47(1):17-23.

830 10. Cherqui S, Courtoy PJ. The renal Fanconi syndrome in cystinosis: pathogenic insights and

831 therapeutic perspectives. Nature reviews Nephrology. 2017;13(2):115-31.

832 11. Elmonem MA, Veys KR, Soliman NA, van Dyck M, van den Heuvel LP, Levtchenko E.
833 Cystinosis: a review. Orphanet journal of rare diseases. 2016;11:47.
834 12. Wilmer MJ, Schoeber JP, van den Heuvel LP, Levtchenko EN. Cystinosis: practical tools for
835 diagnosis and treatment. Pediatric nephrology. 2011;26(2):205-15.
836 13. David D, Princiero Berlingerio S, Elmonem MA, Oliveira Arcolino F, Soliman N, van den
837 Heuvel B, et al. Molecular Basis of Cystinosis: Geographic Distribution, Functional Consequences of
838 Mutations in the CTNS Gene, and Potential for Repair. Nephron. 2019;141(2):133-46.
839 14. Ivanova EA, van den Heuvel LP, Elmonem MA, De Smedt H, Missiaen L, Pastore A, et al.
840 Altered mTOR signalling in nephropathic cystinosis. Journal of inherited metabolic disease.
841 2016;39(3):457-64.
842 15. Nevo N, Thomas L, Chhuon C, Andrzejewska Z, Lipecka J, Guillonneau F, et al. Impact of
843 Cystinosin Glycosylation on Protein Stability by Differential Dynamic Stable Isotope Labeling by Amino
844 Acids in Cell Culture (SILAC). Molecular & cellular proteomics : MCP. 2017;16(3):457-68.
845 16. Sansanwal P, Sarwal MM. p62/SQSTM1 prominently accumulates in renal proximal tubules in
846 nephropathic cystinosis. Pediatric nephrology. 2012;27(11):2137-44.
847 17. Luciani A, Festa BP, Chen Z, Devuyst O. Defective autophagy degradation and abnormal tight
848 junction-associated signaling drive epithelial dysfunction in cystinosis. Autophagy. 2018;14(7):1157-9.
849 18. Sansanwal P, Sarwal MM. Abnormal mitochondrial autophagy in nephropathic cystinosis.
850 Autophagy. 2010;6(7):971-3.
851 19. Zhang W, Li X, Wang S, Chen Y, Liu H. Regulation of TFEB activity and its potential as a
852 therapeutic target against kidney diseases. Cell death discovery. 2020;6:32.
853 20. Johnson JL, Napolitano G, Monfregola J, Rocca CJ, Cherqui S, Catz SD. Upregulation of the
854 Rab27a-dependent trafficking and secretory mechanisms improves lysosomal transport, alleviates
855 endoplasmic reticulum stress, and reduces lysosome overload in cystinosis. Molecular and cellular
856 biology. 2013;33(15):2950-62.

857 21. Sansanwal P, Yen B, Gahl WA, Ma Y, Ying L, Wong LJ, et al. Mitochondrial autophagy
858 promotes cellular injury in nephropathic cystinosis. Journal of the American Society of Nephrology :
859 JASN. 2010;21(2):272-83.
860 22. Raggi C, Luciani A, Nevo N, Antignac C, Terryn S, Devuyst O. Dedifferentiation and aberrations
861 of the endolysosomal compartment characterize the early stage of nephropathic cystinosis. Human
862 molecular genetics. 2014;23(9):2266-78.
863 23. Sansanwal P, Li L, Sarwal MM. Inhibition of intracellular clusterin attenuates cell death in
864 nephropathic cystinosis. Journal of the American Society of Nephrology : JASN. 2015;26(3):612-25.
865 24. Le BL, Iwatani S, Wong RJ, Stevenson DK, Sirota M. Computational discovery of therapeutic
866 candidates for preventing preterm birth. JCI insight. 2020;5(3).
867 25. Naguib YM. Antioxidant activities of astaxanthin and related carotenoids. J Agric Food Chem.
868 2000;48(4):1150-4.
869 26. Ambati RR, Phang SM, Ravi S, Aswathanarayana RG. Astaxanthin: sources, extraction, stability,
870 biological activities and its commercial applications--a review. Mar Drugs. 2014;12(1):128-52.
871 27. Petri D, Lundebye AK. Tissue distribution of astaxanthin in rats following exposure to graded
872 levels in the feed. Comp Biochem Physiol C Toxicol Pharmacol. 2007;145(2):202-9.
873 28. Guo SX, Zhou HL, Huang CL, You CG, Fang Q, Wu P, et al. Astaxanthin attenuates early acute
874 kidney injury following severe burns in rats by ameliorating oxidative stress and mitochondrial-related
875 apoptosis. Mar Drugs. 2015;13(4):2105-23.
876 29. Qiu X, Fu K, Zhao X, Zhang Y, Yuan Y, Zhang S, et al. Protective effects of astaxanthin against
877 ischemia/reperfusion induced renal injury in mice. J Transl Med. 2015;13:28.
878 30. Gahl WA, Balog JZ, Kleta R. Nephropathic cystinosis in adults: natural history and effects of oral
879 cysteamine therapy. Ann Intern Med. 2007;147(4):242-50.
880 31. Reimand J, Isserlin R, Voisin V, Kucera M, Tannus-Lopes C, Rostamianfar A, et al. Pathway
881 enrichment analysis and visualization of omics data using g:Profiler, GSEA, Cytoscape and
882 EnrichmentMap. Nature protocols. 2019;14(2):482-517.

883 32. Futai M, Sun-Wada GH, Wada Y, Matsumoto N, Nakanishi-Matsui M. Vacuolar-type ATPase: A
884 proton pump to lysosomal trafficking. Proceedings of the Japan Academy Series B, Physical and
885 biological sciences. 2019;95(6):261-77.
886 33. Vasanthakumar T, Rubinstein JL. Structure and Roles of V-type ATPases. Trends in biochemical
887 sciences. 2020;45(4):295-307.
888 34. Teplova VV, Tonshin AA, Grigoriev PA, Saris NE, Salkinoja-Salonen MS. Bafilomycin A1 is a
889 potassium ionophore that impairs mitochondrial functions. Journal of bioenergetics and biomembranes.
890 2007;39(4):321-9.
891 35. Gluck SL, Iyori M, Holliday LS, Kostrominova T, Lee BS. Distal urinary acidification from
892 Homer Smith to the present. Kidney international. 1996;49(6):1660-4.
893 36. Zimolo Z, Montrose MH, Murer H. H+ extrusion by an apical vacuolar-type H(+)-ATPase in rat
894 renal proximal tubules. The Journal of membrane biology. 1992;126(1):19-26.
895 37. Wagner CA, Finberg KE, Breton S, Marshansky V, Brown D, Geibel JP. Renal vacuolar H+-
896 ATPase. Physiological reviews. 2004;84(4):1263-314.
897 38. Hennings JC, Picard N, Huebner AK, Stauber T, Maier H, Brown D, et al. A mouse model for
898 distal renal tubular acidosis reveals a previously unrecognized role of the V-ATPase a4 subunit in the
899 proximal tubule. EMBO molecular medicine. 2012;4(10):1057-71.
900 39. Forestier L, Jean G, Attard M, Cherqui S, Lewis C, van't Hoff W, et al. Molecular
901 characterization of CTNS deletions in nephropathic cystinosis: development of a PCR-based detection
902 assay. American journal of human genetics. 1999;65(2):353-9.
903 40. Sakai S, Nishida A, Ohno M, Inatomi O, Bamba S, Sugimoto M, et al. Astaxanthin, a xanthophyll
904 carotenoid, prevents development of dextran sulphate sodium-induced murine colitis. J Clin Biochem
905 Nutr. 2019;64(1):66-72.
906 41. Yang JP, Shin JH, Seo SH, Kim SG, Lee SH, Shin EH. Effects of Antioxidants in Reducing
907 Accumulation of Fat in Hepatocyte. International journal of molecular sciences. 2018;19(9).

908 42. Wang CM, Cai XL, Wen QP. Astaxanthin reduces isoflurane-induced neuroapoptosis via the
909 PI3K/Akt pathway. Mol Med Rep. 2016;13(5):4073-8.
910 43. Qiao J, Rong L, Wang Z, Zhang M. Involvement of Akt/GSK3beta/CREB signaling pathway on
911 chronic omethoate induced depressive-like behavior and improvement effects of combined lithium
912 chloride and astaxanthin treatment. Neurosci Lett. 2017;649:55-61.
913 44. Deng X, Wang M, Hu S, Feng Y, Shao Y, Xie Y, et al. The Neuroprotective Effect of
914 Astaxanthin on Pilocarpine-Induced Status Epilepticus in Rats. Front Cell Neurosci. 2019;13:123.
915 45. Kim JH, Nam SW, Kim BW, Choi W, Lee JH, Kim WJ, et al. Astaxanthin improves stem cell
916 potency via an increase in the proliferation of neural progenitor cells. Int J Mol Sci. 2010;11(12):5109-19.
917 46. Kim JH, Nam SW, Kim BW, Kim WJ, Choi YH. Astaxanthin improves the proliferative capacity
918 as well as the osteogenic and adipogenic differentiation potential in neural stem cells. Food Chem
919 Toxicol. 2010;48(6):1741-5.
920 47. Zhang H, Yang W, Li Y, Hu L, Dai Y, Chen J, et al. Astaxanthin ameliorates cerulein-induced
921 acute pancreatitis in mice. Int Immunopharmacol. 2018;56:18-28.
922 48. Chitchumroonchokchai C, Bomser JA, Glamm JE, Failla ML. Xanthophylls and alpha-tocopherol
923 decrease UVB-induced lipid peroxidation and stress signaling in human lens epithelial cells. J Nutr.
924 2004;134(12):3225-32.
925 49. Yan T, Zhao Y, Zhang X, Lin X. Astaxanthin Inhibits Acetaldehyde-Induced Cytotoxicity in SH-
926 SY5Y Cells by Modulating Akt/CREB and p38MAPK/ERK Signaling Pathways. Mar Drugs. 2016;14(3).
927 50. Ikeda Y, Tsuji S, Satoh A, Ishikura M, Shirasawa T, Shimizu T. Protective effects of astaxanthin
928 on 6-hydroxydopamine-induced apoptosis in human neuroblastoma SH-SY5Y cells. J Neurochem.
929 2008;107(6):1730-40.
930 51. Wang HQ, Sun XB, Xu YX, Zhao H, Zhu QY, Zhu CQ. Astaxanthin upregulates heme
931 oxygenase-1 expression through ERK1/2 pathway and its protective effect against beta-amyloid-induced
932 cytotoxicity in SH-SY5Y cells. Brain Res. 2010;1360:159-67.

933 52. Lin X, Zhao Y, Li S. Astaxanthin attenuates glutamate-induced apoptosis via inhibition of
934 calcium influx and endoplasmic reticulum stress. Eur J Pharmacol. 2017;806:43-51.
935 53. Bhuvaneswari S, Yogalakshmi B, Sreeja S, Anuradha CV. Astaxanthin reduces hepatic
936 endoplasmic reticulum stress and nuclear factor-kappaB-mediated inflammation in high fructose and high
937 fat diet-fed mice. Cell Stress Chaperones. 2014;19(2):183-91.
938 54. Kitahara A, Takahashi K, Morita N, Murashima T, Onuma H, Sumitani Y, et al. The Novel
939 Mechanisms Concerning the Inhibitions of Palmitate-Induced Proinflammatory Factor Releases and
940 Endogenous Cellular Stress with Astaxanthin on MIN6 beta-Cells. Mar Drugs. 2017;15(6).
941 55. Ishiki M, Nishida Y, Ishibashi H, Wada T, Fujisaka S, Takikawa A, et al. Impact of divergent
942 effects of astaxanthin on insulin signaling in L6 cells. Endocrinology. 2013;154(8):2600-12.
943 56. Feng W, Wang Y, Guo N, Huang P, Mi Y. Effects of Astaxanthin on Inflammation and Insulin
944 Resistance in a Mouse Model of Gestational Diabetes Mellitus. Dose Response.
945 2020;18(2):1559325820926765.
946 57. Jefferies KC, Cipriano DJ, Forgac M. Function, structure and regulation of the vacuolar (H+)-
947 ATPases. Archives of biochemistry and biophysics. 2008;476(1):33-42.
948 58. Zoncu R, Bar-Peled L, Efeyan A, Wang S, Sancak Y, Sabatini DM. mTORC1 senses lysosomal
949 amino acids through an inside-out mechanism that requires the vacuolar H(+)-ATPase. Science.
950 2011;334(6056):678-83.
951 59. Coffey EE, Beckel JM, Laties AM, Mitchell CH. Lysosomal alkalization and dysfunction in
952 human fibroblasts with the Alzheimer's disease-linked presenilin 1 A246E mutation can be reversed with
953 cAMP. Neuroscience. 2014;263:111-24.
954 60. Hughes AL, Gottschling DE. An early age increase in vacuolar pH limits mitochondrial function
955 and lifespan in yeast. Nature. 2012;492(7428):261-5.
956 61. Kleta R, Bernardini I, Ueda M, Varade WS, Phornphutkul C, Krasnewich D, et al. Long-term
957 follow-up of well-treated nephropathic cystinosis patients. The Journal of pediatrics. 2004;145(4):555-60.

958 62. Nesterova G, Williams C, Bernardini I, Gahl WA. Cystinosis: renal glomerular and renal tubular
959 function in relation to compliance with cystine-depleting therapy. Pediatric nephrology. 2015;30(6):945-
960 51.
961 63. Wilmer MJ, Willems PH, Verkaart S, Visch HJ, de Graaf-Hess A, Blom HJ, et al. Cystine
962 dimethylester model of cystinosis: still reliable? Pediatric research. 2007;62(2):151-5.
963 64. Grahammer F, Haenisch N, Steinhardt F, Sandner L, Roerden M, Arnold F, et al. mTORC1
964 maintains renal tubular homeostasis and is essential in response to ischemic stress. Proceedings of the
965 National Academy of Sciences of the United States of America. 2014;111(27):E2817-26.
966 65. Marchi S, Patergnani S, Pinton P. The endoplasmic reticulum-mitochondria connection: one
967 touch, multiple functions. Biochimica et biophysica acta. 2014;1837(4):461-9.
968 66. Farmer BC, Walsh AE, Kluemper JC, Johnson LA. Lipid Droplets in Neurodegenerative
969 Disorders. Frontiers in neuroscience. 2020;14:742.
970 67. Li PF, Dietz R, von Harsdorf R. p53 regulates mitochondrial membrane potential through reactive
971 oxygen species and induces cytochrome c-independent apoptosis blocked by Bcl-2. The EMBO journal.
972 1999;18(21):6027-36.
973 68. Oda E, Ohki R, Murasawa H, Nemoto J, Shibue T, Yamashita T, et al. Noxa, a BH3-only
974 member of the Bcl-2 family and candidate mediator of p53-induced apoptosis. Science.
975 2000;288(5468):1053-8.
976 69. Moran A, Ben-Nun A, Potashnik R, Bashan N. Renal cells in culture as a model for cystinosis.
977 Journal of basic and clinical physiology and pharmacology. 1990;1(1-4):357-72.
978 70. Uniyal AP, Mansotra K, Yadav SK, Kumar V. An overview of designing and selection of
979 sgRNAs for precise genome editing by the CRISPR-Cas9 system in plants. 3 Biotech. 2019;9(6):223.
980 71. Tusher VG, Tibshirani R, Chu G. Significance analysis of microarrays applied to the ionizing
981 radiation response. Proceedings of the National Academy of Sciences of the United States of America.
982 2001;98(9):5116-21.
983